ISSN: 2754-4966

Journal of Nanosciences Research & Reports

SCIENTIFIC Research and Community

Research Article

Open Access

Effect of Deposition Time on Material Properties of ZnO Nanorods Grown on GZO Seed Layer by CBD

Ungula J[1,2], Kiprotich S[3]* and Swart HC[1]

[1]Department of Physics, University of the Free State, PO Box 339, Bloemfontein 9300, South Africa

[2]Department of Pure and Applied Sciences, Kenya Methodist University, P.O Box 267, Meru 60200, Kenya

[3]Department of Physical and Biological Sciences, Murang'a University of Technology, P.O Box 75, Murang'a 10200, Kenya

ABSTRACT

ZnO nanorods (ZNRs) were grown on Ga-doped ZnO (GZO) through a two-step procedure, involving pre-treatment to form the seed layer followed by growth of the nanorods through chemical bath deposition (CBD) method. The study determines the effect of different growth deposition times (ranging between 30 and 150 min) at 90°C growth temperature and 0.05M concentration of precursor solution. The influence of this growth parameter on structural and optical properties of ZNRs thin films is presented. The pattern of X-ray diffraction displayed ZNRs thin films with a polycrystalline hexagonal structure. The estimated crystallite size increased with deposition time while the calculated strain was found to decrease with increase in time, an implication of improved crystallinity at longer deposition time as displayed by highest XRD peak intensity at 90 min. The scanning electron microscopy and atomic force microscopy images exhibited various types of morphologies at different deposition time with homogenously distributed nanorods observed at 90 min. An inverse relation between the optical band gaps and deposition growth time of the prepared nanorods was observed. The ZNRs sample grown on the transparent conductive film of GZO, with high luminescence and perfect crystallization produced at the 90 min growth deposition time could suitable for use as a photoanode component of the dye-sensitized solar cell.

Corresponding author

Sharon Kiprotich, Department of Physical and Biological Sciences, Murang'a University of Technology, P.O Box 75, Murang'a 10200, Kenya.

Received: January 05, 2024; **Accepted:** January 12, 2024; **Published:** January 22, 2024

Keywords: ZnO Nanorods, Thin Films, Crystal Structure, CBD, Spin Coating

Introduction

One-dimensional (1D) nanostructures such as nanotubes, nanoribbons, nanowires, nanorods, nanocables, and nanobelts have taken centre stage in the past few years, this came after the carbon nanotubes was discovered [1-5]. The 1D nanostructures have inspired immense research in the field of science because they exhibit excellent optical, and electrical properties which are displayed in their vast applications in various nanodevices owing to their large surface area.

Many reports have described ZnO nanorods (ZNRs) preparation using one-step aqueous method such as pulsed laser deposition, chemical vapor deposition and electrochemical deposition [6-8]. Complicated procedures, high temperatures, and sophisticated equipment are reported to have been used in the mentioned methods of ZNRs synthesis. The chemical bath deposition (CBD) method, on the other hand, is quite a facile and inexpensive process which requires simple apparatus and most importantly, the nanorods can be grown at low temperatures [9, 10]. Additionally, the shape and size of the ZNRs can easily be controlled using the CBD technique by fine-tuning the growth parameters such as stoichiometric ratios of the reagents, solution concentration, growth temperature, growth time, and pH of the solution [11-13]. As far as the CBD technique is concerned, controlling the size and morphology of the nanorods has proven to be challenging that is why most researchers use a two-step process which involves pretreatment of the substrates and chemical bath deposition process [14, 15]. Study reports that the ZNRs grown on Si substrate through CBD method displayed poor results and difficulty in reproducibility [16]. It is, thus, commonly agreed that ZnO seeding, by spin coating or sputtering, is essential for easy and convenient growth of a well-aligned ZNRs perpendicular to the substrates [17, 18].

Ga-doped ZnO (GZO) is identified in this study, as transparent conducting oxide seed layer because, it does not easily undergo oxidation like aluminium and due to the fact that ionic and covalent radii of Ga and Zn are pretty close [19]. We believe, achieving control over the properties and characteristics of ZNRs through the seed layer doping has not been widely reported in literature. The report of this study will add to the body of knowledge on ways of improving the versatile properties of ZNRs deposited on the GZO transparent oxide seed layer. A promising combination to be employed for use as photoelectrode in dye-sensitized solar cells application. Indeed, ZNRs show distinct morphologies in different deposition growth times with well-aligned rods obtained at 90 min.

Experimental Procedure

The reagents used are zinc nitrate hexahydrate (Zn $(NO_3)_2.6H_2O$, 99.9% purity), sodium hydroxide (NaOH), gallium nitrate hexahydrate ($Ga(NO_3)_3.6H_2O$, 99.9% purity), HMTA ($C_6H_{12}N_4$, 99.9% purity) and distilled water. The reagents are all of analytical grade so no further refinement was not required. ZnO nanorods were grown on the GZO seed layer through a two-step CBD method.

Firstly, as prepared and optimized GZO nanoparticles were spin-coated on glass substrate to make a seed layer. The GZO nanopowders were prepared as described [20]. The GZO powder was ground, dissolved in suitable solvent and mixed into a homogenous paste to form the spin coating solution. SPEN 150 spin coater operating at 2000 rpm for 30s was used to spin-coat the solution on the glass substrate and the film so formed pre-annealed on a hot plate for 10min at 250 °C. The GZO thin film deposition and pre-heating procedures were done repeatedly 10 times to obtain suitable thickness and uniform coverage of the seed layer and eventually post annealed using a furnace in air from room temperature (RT) to 500 °C for 120 min duration. Secondly, the GZO seeded-substrate was immersed in reaction bath of precursor solutions to achieve growth of the ZNRs. The reaction bath was formed by dissolving 0.05 equimolar solutions of Zn $(NO_3)_2$). $6H_2O$ and HMTA in distilled water in a 100 ml beaker at RT. To this, the reaction vessel containing the reaction bath and the seeded glass substrate was placed in a thermostatically controlled water bath. To monitor the growth process in CBD set up, the deposition growth time was varied from 30-150 min. Finally, the glass substrate film was removed from the reaction vessel, and rinsing was done using running water and thereafter left to dry in an oven at 70°C for about 5 min.

Various measurements were conducted on the as grown ZNRs. The crystal structures were examined by X-ray diffraction (XRD) sing a Bruker D8-Advance X-ray diffractometer (with monochromatic CuKα radiation, λ=1.5406 Å). Scanning electron microscope (SEM, JEOL JSM-7800F) was used to characterize the morphology, and accompanying Oxford Aztec EDS (Energy-dispersive X-ray spectroscopy) measured the elemental composition of the products. An atomic force microscope (AFM, Shimadzu SPM – 9600) was used to study surface topography. The optical emission spectra were measured on a UV–Vis-IR spectroscopy (Perkin Elmer Lambda 950). While the photoluminescence (PL) spectroscopy studies were conducted by means of a Cary Eclipse fluorescence spectrophotometer; model LS-55.

Results and Discussion

XRD Analysis

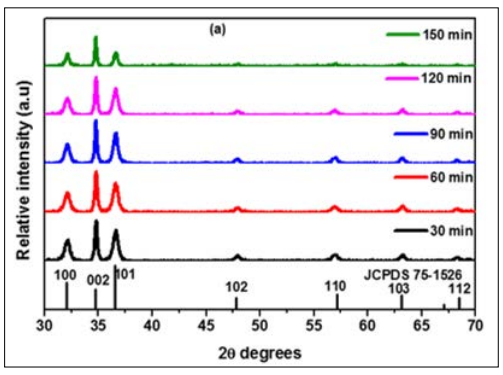

Figure 1(a): XRD Patterns of ZNRs on GZO Seeded Glass Substrate in an Equimolar Precursor Solution at Different Deposition Times.

Figure 1(a) displays the XRD patterns of the ZnO NRs thin films grown on GZO seeded glass substrate for varied deposition times (30 -150 min. All patterns reveal the distinct diffraction peaks which are characteristic of the hexagonal crystal structure well indexed to the JCPDS card No. 75-1526, a = 3.220 nm, and c = 5.200 nm of ZnO, corresponding to the [100], [002], [101], [102], [110], [103] and [112] planes. The XRD spectra of ZNRs show general enhancement of peak intensities indicative of an improvement in crystallinity. The diffraction peak intensity increased to a maximum at 90 min and decreased for longer deposition time. No other characteristic peaks from the XRD pattern could be identifiedwhich confirms high level crystrallization of the samples and existence of only single phase of hexagonal ZnO wurtzite structure.

Clearly, as could be seen in Figure 1(a), the intensity of [002] plane is the most enhanced as compared to the usual [101] most intense reflection in the standard pattern of ZnO. This observed phenomenon indicates a preferred growth of ZNRs along the c-axis [21]. More often, to characterize the orientation of ZNRs, intensity ratios of (002) and (101) planes is used because it is [002] plane only which can give any further information and evidence on the preferred c-axis orientation of ZNRs. Thus, the degree of c-orientation described by the relative texture coefficient (*TC*) was calculated using the expression [22].

The calculated values of *TC* for (002) and (101) diffraction peaks denoted as $TC_{(002)}$ and $TC_{(101)}$ respectively for different deposition times are presented in Figure 1(b).

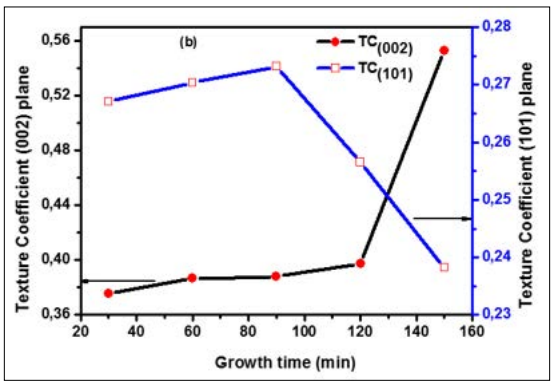

Figure 1(b): The Texture Coefficients of [002] and [101] Planes of ZNRs Arrays as a Function of Growth Time.

Figure 1(b) shows that the *TC* values of (002) planes are greater than that of (101) planes confirming the preferential growth of the ZNRs in the c-axis as mentioned earlier. The growth along this direction is favored because any growth deviating from c-axis get obstructed due to high density of the nanostructures [23]. The NRs, therefore, are pertinent to grow along the c-axis when competition and optimization of rules are put into consideration. Studies have shown that the [101] surface face grows the fastest in nanopowders, as the growth progresses. However, the [002] plane in NRs thin films grows faster and increase in orientation at the expense of the [101] plane due to higher rates of deposition and growth along the c-axis resulting in reduced growth along the [101] orientation [24]. It is also vital to note that the *TC* values of (002) plane increases as the deposition time increase. Similarly, the *TC* values of (101) plane increased, albeit, up to 90 min of deposition time and declined thereafter.

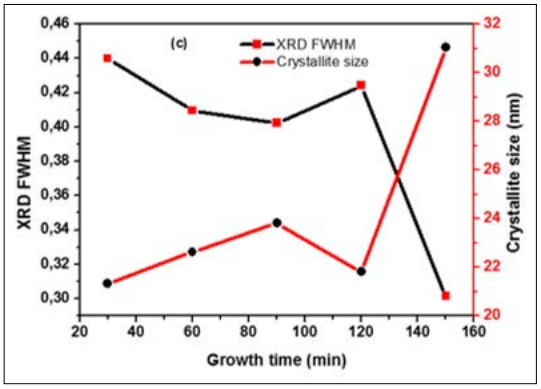

Figure 1(c): Illustration of Crystallite Size and Variation of FWHM of ZNRs Diffraction Peaks Against Deposition Growth Time.

The full width at half maximum (FWHM) of the as-prepared ZNRs thin films was obtained from all the diffraction peaks. It was found that FWHM values decreased with increase in deposition time as displayed in Figure 1(c). These FWHM values were then used in calculation of crystallite sizes of characterized samples using Debye Scherrer formula [25]. The sizes of the crystallites were found to increase as the deposition time increase (30 - 150 min) as shown in Figure 1(c). The estimated crystallite sizes were 21.31, 22.62, 23.81, 21.81 and 31.04 nm for 30, 60, 90, 120 and 150 min of deposition time respectively.

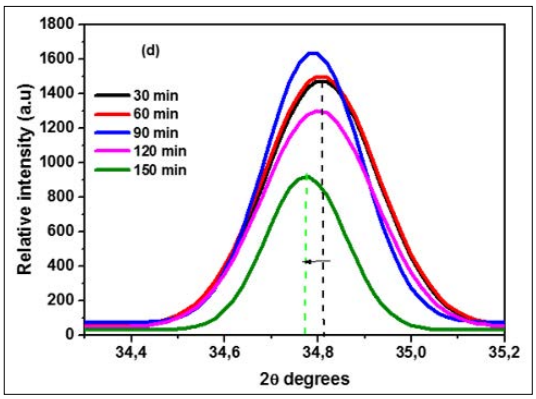

Figure 1(d): A Magnified XRD Pattern of Diffraction Peak Displaying Peak Position Shift and Change in Peak Intensity for the ZNRs at Different Deposition Growth Time.

With an increase in deposition time, peaks shift to lower 2θ angle was observed in the diffraction planes of ZNRs (Figure 1(d)). This shift to lower diffraction angle, attributed to lattice expansion, is a further confirmation of an increase in the crystallite size with increase in deposition time. The verification of expansion of lattice parameters of ZNRS was done by calculating the values of dominant diffracted peaks of the XRD spectra and tabulated in table 1 [26]. To compare the value of bulk ZnO (c = 5.204 Å), the calculated values are slightly lower demonstrating that the characterized samples may be under some strain.

The Williamson-Smallman equation, was also used to establish the internal strain (ε) of the nanorods and results shown in Table 1[27].

$$\varepsilon = \frac{\beta}{4\tan\theta} \quad (1)$$

Where, θ is the angle of diffraction and β is the FWHM.

Similarly, calculation of the lengths of the dislocation density (δ) was established using equation (2) [28];

$$\delta = \frac{1}{D^2} \quad (2)$$

Where D is the crystal size obtained from the XRD pattern.

Table 1: A table displaying the lattice constant, the AFM RMS values and particle sizes, crystallite size, [002] plane peak position, strain and dislocation density of ZNRs at the different cell at varied deposition growth time.

Growth time (min)	Lat. Constants (Å)			AFM analysis		Crystallite			D/density
	a	c	c/a ratio	R.M.S (nm)	Size (nm)	size (nm)	Peak [002]	Strain (ε)	δ (M^{-2})
30	3.2140	5.19819	1.6174	4.9	33.3	21.31	34.81	0.000606	0.0022
60	3.2141	5.20129	1.6183	-	-	22.62	34.8	0.000553	0.00195
90	3.2144	5.20215	1.6184	6.1	39.6	23.81	34.79	0.000543	0.00176
120	3.2140	5.16915	1.6083	-	-	21.81	34.8	0.000573	0.0021
150	3.2149	5.20115	1.6178	9.5	95.0	31.04	34.78	0.000407	0.001

It could be deduced from Table 1, that both the values of the strain and the dislocation density were inversely related to the deposition growth time. The dislocation density gives an indication of the dislocation network in the structure of the particle, therefore the decrease with increase in the deposition growth time indicate improved crystallinity.

SEM Observations

The SEM micrograph images of ZNRs at different deposition times are presented in Figure 2. As shown, remarkable morphological transformations and improvements have been observed on the as-prepared ZNRs thin films as the time increases. For the shorter duration of deposition, tiny and agglomerated mixtures of nanorods and nanospheres could be seen which changed into well-aligned and uniformly distributed ZNRs at 90 min. The film deposited at longer deposition time, however, showed an enlarged morphology of flower-like structures of ZNRs.

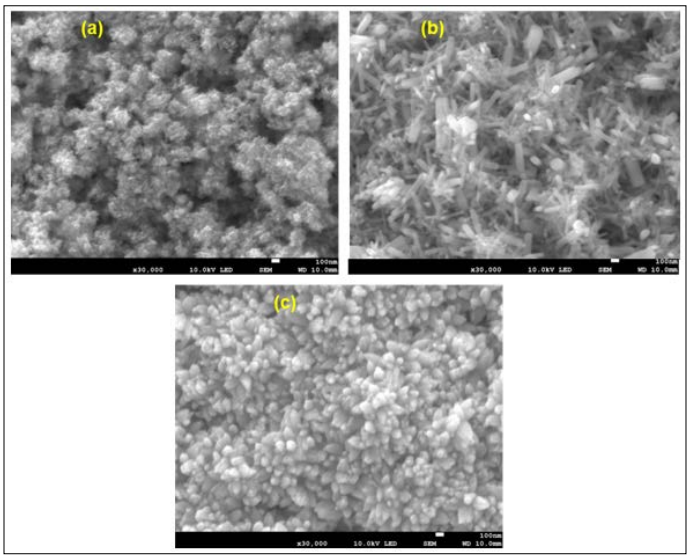

Figure 2: SEM Images of ZNRs Prepared at Deposition Times(a) 30, (b) 90 and (c) 150 min

Apparently, at shorter deposition time nucleation takes place where the growth mechanism processes (diffusion and aggregation) occur as explained [29]. Furthermore, the differences in morphology, density, orientation and alignment of ZNRs can be further explained in view of the formation mechanism that governs CBD method where solid phase is formed on a substrate from an aqueous solution through nucleation and growth processes [30]. As the growth time progressed, the dimensions of the nanorods increased but stopped after some period of time and erosion process began resulting to change in morphology of the ZNRs [31].

AFM Analysis

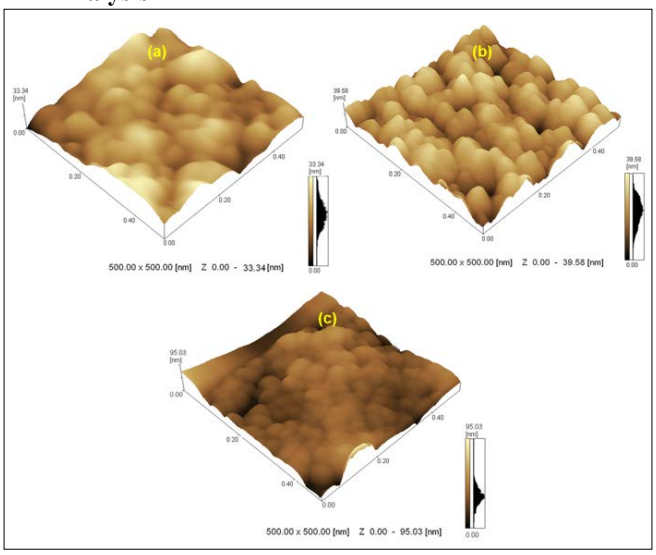

Figure 3: AFM 3-D Images of ZNRs Prepared at Deposition Times (a) 30, (b) 90 and (c) 150 min

In order to further the study of the surface topography of the ZNRs thin films prepared on GZO seeded glass substrate, atomic force microscopy (AFM) technique was utilized. Figures. 3(a-c) display 3-D AFM images of ZNRs covering 500 x 500 nm^2 prepared at different deposition times. They display clear changes in surface topography as the deposition time is increased which further confirms the observation made with the SEM images. The ZNRs thin films prepared at 90 min showed more defined, well-aligned and homogeneously distributed nanorods over the all surface of the substrate. The root mean square (RMS) roughness of the ZNRs were 4.86, 6.07 and 9.46 nm for the deposition time of 30, 90 and 150 min respectively. The observed increase in film roughness is attributed to the increase in grain size of particles (33.34, 39.58 and 95.03 nm for 30, 90 and 150 min of growth time) [32].

Photoluminescence Analysis

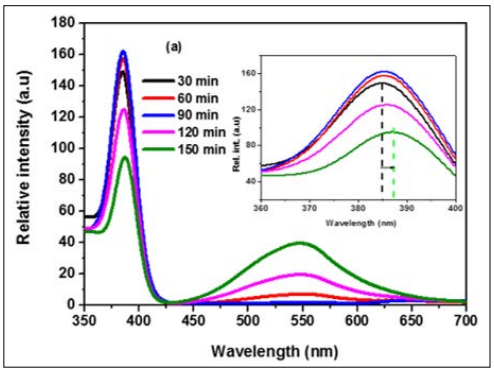

Figure 4(a): Room-Temperature PL Spectra and Inset: Enlarged Excitonic Peak Emission Spectra for ZNRs Grown at Various Deposition Times.

The PL spectra of the ZNRs thin films at different growth times are displayed in Figure 4(a). There are two PL emissions observed; one around 385 nm and the second one around 550 nm. The blue emission peaks also called excitonic peak emission (around 385 nm) is known to be associated with the recombination of the free excitons of ZnO. Whereas, the PL emission peaks around ~550 nm is attributed to defects such as O and Zn vacancies [33-36]. The enhancement of the excitonic peak emission was observed when deposition time was increased and reached a maximum at 90 min but decreased thereafter, as illustrated in Figure 4(b). The decline in excitonic emission, with the increase in time, could be due to increased concentration of deep level defects [20]. This indicates that best crystallinity can be obtained at 90 min of deposition time which is in agreement with the XRD observation. As shown in the PL spectra, Figure 4(a) inset, notably the excitonic peak emission of the ZNRs shifts towards higher wavelengths (385-387 nm) with the increase in deposition time (30-150 min). The observed red-shift could be as a result of growth of the particles as explained by Ostwald ripening process where large particles overtake the growth of small particles [30, 37].

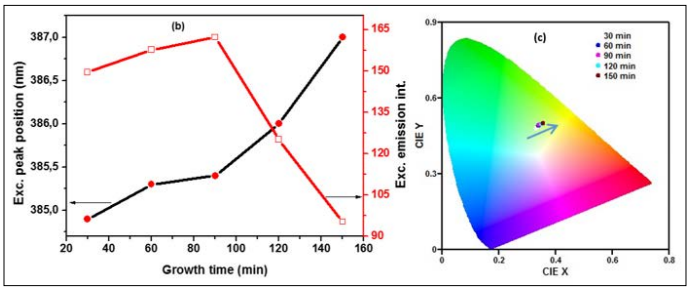

Figure 4(b): Variation in the Excitonic Peak Position and Peak Intensities
Figure 4(c): CIE Image Displaying Colour Changes with Deposition Time

The Commission International de I'Eclairage (CIE) chromaticity image of the as-prepared ZNRs was drawn and shown in Figure 4(c). The color emission of the ZNRs prepared in the study is described by the x, and y coordinates of CIE. The CIE diagram confirms the findings from the PL which indicate a red shift in emission when the deposition time progressed from 30-90 min.

UV-V is Spectral Study

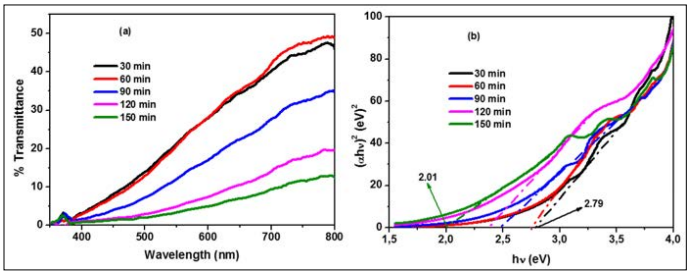

Figure 5(a): UV–V is % Transmittance
Figure 5(b): Band Gap Plot of ZNRs at Different Deposition Times

The fraction of an incident light of a specific wavelength which passes through a sample is what is referred to as transmittance. The transmittance spectra of ZNRs grown at different deposition times are depicted in Figure 5(a). The spectra display high transparency in the wavelength range 500-800 nm for all the prepared samples.

The ZnO transparency property in the visible region is thought to be due to the possession of wide band gap energy [38]. The variation of transmittance with deposition time was observed. It was noted that the films revealed a decline in transmittance at a prolonged duration of deposition. High transmittance displayed at a shorter duration of growth could be attributed to a thin layer of the film formed. As the growth progresses to longer deposition time, the film becomes dense as larger and longer NRs are formed and hence reducing the % percentage transmittance. Furthermore, a red shift in absorption edges was observed as deposition time is increased from 30-150 min as depicted in Figure 5(a). The shift to a longer wavelength at a prolonged duration of growth could be due to enlargement of grains formed.

The absorption coefficient (α) is calculated from % T data using the Beer-Lambert law eq. (3):

$$\alpha = \frac{1}{d}\ln\left[\frac{1}{T}\right] \quad (3)$$

The α and the incident photon energy (hv) is related by the Tauc's formula eq. (4). In the case of direct allowed transitions such as those found in the direct band gap of ZnO, close to the band edge, α approximates to the equation. The band gap of the material is denoted as Eg.

$$\alpha hv = A\sqrt{hv - Eg} \quad (4)$$

The nature of the band gap transition is said to be direct as could be explained by the linear nature of the plot. The extrapolation of the linear portion of the curve to the energy axis at $hv = 0$, gives the values of the band which was found to decrease with increase in deposition time from 2.79 to 2.01 eV for the ZNRs as shown in Figure 5(b). This phenomenon can be explained to be caused by the increase in the size of the crystallites and alteration of grain borderline arrangements during growth as confirmed by XRD results. The values of band gaFfigfigp energies obtained in this study agree with those reported by Ajuba et al (2010) [39, 40]. Variation in the values of band gap of the ZNRs films with deposition time offers an easy way to engineer both the structural and optical properties to suit a specific application.

Conclusions

ZNRs thin films were successfully produced on GZO seeded substrate by the two-step CBD technique at different deposition times while keeping growth temperature and precursor concentrations constant. XRD analysis displayed a wurtzite structure with a preferred [002] plane orientation with the NRs growing along the c-axis. Increase in crystallite sizes calculated from the Scherrer's formula with an increase in deposition time was observed. SEM and AFM images showed a variation of surface morphologies with deposition time with well aligned NRs obtained at 90 min of growth time. The PL excitonic peak intensity was found to increase to a maximum at 90 min and decreases thereafter for a longer duration of growth due to increase in defects in the samples. The ZNRs sample obtained at 90 min was confirmed, by the analysis techniques, to possess the best structural and optical properties hence the recommended deposition time for the preparation of the nanorods by CBD on the GZO substrate.

Acknowledgement

The financial support from the University of the Free State is recognized.

Declaration of Conflict of Interest

The authors declare no conflict of interest.

References

1. Iijima S (1991) Helical microtubules of graphitic carbon. Nature 354: 56-58.
2. Huang MH, Wu Y, Feick H, Tran N, Weber E, et al. (2001) Catalytic growth of zinc oxide nanowires by vapor transport. Advanced materials 13: 113-116.
3. Li JY, Chen XL, Li H, He M, Qiao ZY (2001) Fabrication of zinc oxide nanorods. Journal of crystal growth 233: 5-7.
4. Pan ZW, Dai ZR, Wang ZL (2001) Nanobelts of semiconducting oxides. Science 291: 1947-1949.
5. Wu JJ, Liu SC, Wu CT, Chen KH, Chen LC (2002) Heterostructures of ZnO–Zn coaxial nanocables and ZnO nanotubes. Applied Physics Letters 81: 1312-1314.
6. Huang MH, Mao S, Feick H, Yan H, Wu Y, et al. (2001) Room-temperature ultraviolet nanowire nanolasers. Science 292: 1897-1899.
7. Sun Y, Fuge GM, Ashfold MN (2004) Growth of aligned ZnO nanorod arrays by catalyst-free pulsed laser deposition methods. Chemical Physics Letters 396: 21-26.
8. Park WI, Kim DH, Jung SW, Yi GC (2002) Metalorganic vapor-phase epitaxial growth of vertically well-aligned ZnO nanorods. Applied Physics Letters 80: 4232-4234.
9. Yu H, Zhang Z, Han M, Hao X, Zhu F (2005) A general low-temperature route for large-scale fabrication of highly oriented ZnO nanorod/nanotube arrays. Journal of the American Chemical Society 127: 2378-2379.
10. Vayssieres L, Keis K, Lindquist SE, Hagfeldt A (2001) Purpose-built anisotropic metal oxide material: 3D highly oriented microrod array of ZnO. The Journal of Physical Chemistry B 105: 3350-3352.
11. Vernardou D, Kenanakis G, Couris S, Koudoumas E, Kymakis E, et al. (2007) pH effect on the morphology of ZnO nanostructures grown with aqueous chemical growth. Thin solid films 515: 8764-8767.
12. Zhang H, Yang D, Li S, Ma X, Ji Y, et al. (2005) Controllable growth of ZnO nanostructures by citric acid assisted hydrothermal process. Materials Letters 59: 1696-1700.
13. Zhaochun Z, Baibiao H, Yongqin Y, Deliang C (2001) Electrical properties and Raman spectra of undoped and Al-doped ZnO thin films by metalorganic vapor phase epitaxy. Materials Science and Engineering: B 86: 109-112.
14. Vayssieres L (2003) Growth of arrayed nanorods and nanowires of ZnO from aqueous solutions. Advanced Materials 15: 464-466.
15. Peterson RB, Fields CL, Gregg BA (2004) Epitaxial chemical deposition of ZnO nanocolumns from NaOH solutions. Langmuir 20: 5114-5118.
16. Yang LL (2010) Synthesis and Characterization of ZnO nanostructures (Doctoral dissertation, Linköping University Electronic Press) http://www.diva-portal.org/smash/record.jsf?pid=diva2%3A359293&dswid=4482.
17. Wang SF, Tseng TY, Wang YR., Wang CY, Lu HC (2009) Effect of ZnO seed layers on the solution chemical growth of ZnO nanorod arrays. Ceramics International 35: 1255-1260.
18. Cui JB, Daghlian CP, Gibson UJ, Püsche R, Geithner P, et al. (2005) Low-temperature growth and field emission of ZnO nanowire arrays. Journal of Applied Physics 97: 044315
19. Ungula J, Dejene BF, Swart HC (2018) Band gap engineering, enhanced morphology and photoluminescence of un-doped, Ga and/or Al-doped ZnO nanoparticles by reflux precipitation method. Journal of Luminescence 195: 54-60.

20. Ungula J, Dejene BF (2016) Effect of solvent medium on the structural, morphological and optical properties of ZnO nanoparticles synthesized by the sol–gel method. Physica B: Condensed Matter 480: 26-30.
21. Yi GC, Wang C, Park WI (2005) ZnO nanorods: synthesis, characterization and applications. Semiconductor science and technology 20: 22-34.
22. Rusu DI, Rusu GG, Luca D (2011) Structural Characteristics and Optical Properties of Thermally Oxidized Zinc Films. Acta Physica Polonica Series A 119 DOI: 10.12693/APhysPolA.119.850.
23. Wu WY, Yeh CC, Ting JM (2009) Effects of seed layer characteristics on the synthesis of ZnO nanowires. Journal of the American Ceramic Society 92: 2718-2723.
24. Yang J, Lang J, Yang L, Zhang Y, Wang D, et al. (2008) Low-temperature growth and optical properties of ZnO nanorods. Journal of Alloys and Compounds 450: 521-524.
25. Cullity BD, Stock SR (2001) Elements of x-ray diffraction, Prentice Hall. Upper Saddle River, NJ, 388.
26. Kumari V, Vinod Kumar, Malik BP, Mehra RM, Mohan D (2012) Nonlinear optical properties of erbium doped zinc oxide (EZO) thin films. Optics Communications 285: 2182-2188.
27. Lalitha S, Sathyamoorthy R, Senthilarasu S, Subbarayan A, Natarajan K (2004) Characterization of CdTe thin film-dependence of structural and optical properties on temperature and thickness. Solar energy materials and solar cells 82: 187-199.
28. Purohit A, Chander S, Nehra SP, Dhaka MS (2015) Effect of air annealing on structural, optical, morphological and electrical properties of thermally evaporated CdSe thin films. Physica E: Low-dimensional Systems and Nanostructures 69: 342-348.
29. Kiprotich S, Onani MO, Dejene FB (2018) High luminescent L-cysteine capped CdTe quantum dots prepared at different reaction times. Physica B: Condensed Matter 535: 202-210.
30. Zhao J, Jin ZG, Liu XX, Liu ZF (2006) Growth and morphology of ZnO nanorods prepared from Zn $(NO_3)_2$/NaOH solutions. Journal of the European Ceramic Society 26: 3745-3752.
31. Yang J, Lang J, Yang L, Zhang Y, Wang D, et al. (2008) Low-temperature growth and optical properties of ZnO nanorods. Journal of Alloys and Compounds 450: 521-524.
32. Hasabeldaim E, Ntwaeaborwa OM, Kroon RE, Coetsee E, Swart HC (2017) Effect of substrate temperature and post annealing temperature on ZnO: Zn PLD thin film properties. Optical Materials 74: 139-149.
33. Srikant V, Clarke DR (1998) On the optical band gap of zinc oxide. Journal of Applied Physics 83: 5447-5451.
34. Børseth TM, Svensson BG, Kuznetsov AY, Klason P, Zhao QX, et al. (2006) Identification of oxygen and zinc vacancy optical signals in ZnO. Applied Physics Letters 89: 262112.
35. Tsai CH, Wang WC, Jenq FL, Liu CC, Hung CI, et al. (2008) Surface modification of ZnO film by hydrogen peroxide solution. Journal of applied physics 104: 053521.
36. Lei Z, Lian JS, Liu YH, Jiang Q (2008) Influence of preparation methods on photoluminescence properties of ZnO films on quartz glass. Transactions of Nonferrous Metals Society of China 18: 145-149.
37. Jiang F, Muscat AJ (2012) Ligand-controlled growth of ZnSe quantum dots in water during Ostwald ripening. Langmuir 28: 12931-12940.
38. Lin SS, Huang JL (2004) Effect of thickness on the structural and optical properties of ZnO films by r.f. magnetron sputtering. Surface and Coatings Technology 185: 222-227.
39. Ajuba AE, Ezugwu SC, Ezekoye BA, Ezema FI, Asogwa PU (2010) Influence of pH on the structural, optical and solid state properties of chemical bath deposited ZnO thin films. Journal of Optoelectronics and Biomedical Materials 2: 73-78.
40. Ungula J, Dejene BF, Swart HC (2018) Effect of pH on the structural, optical and morphological properties of Ga-doped ZnO nanoparticles by reflux precipitation method. Physica B: Condensed Matter 535: 251-257.

Copyright: ©2024 Sharon Kiprotich, et al. This is an open-access article distributed under the terms of the Creative Commons Attribution License, which permits unrestricted use, distribution, and reproduction in any medium, provided the original author and source are credited.